Materials Today Communications 50 (2026) 114411

Contents lists available at ScienceDirect

Materials Today Communications

journal homepage: www.elsevier.com/locate/mtcomm

# Mechanical and fracture analysis of polyoxymethylene for industrial, aerospace and automotive structures

Sid Ahmed Reffas [a], R. Yekhlef [b], D. Belfennache [b], M. Fatmi [c,*], M.A. Ghebouli [c,d], S. Alomairy [e], Mustafa Jaipallah Abdelmageed Abualreish [f], Aseel Smerat [g,h]

[a] Department of Engineering Mechanics, University Djilali Liabes of Sidi Bel Abbès, 22000, Algeria
[b] Research Center in Industrial Technologies CRTI, P.O. Box 64, Cheraga, Algiers 16014, Algeria
[c] Research Unit on Emerging Materials (RUEM), University Ferhat Abbas of Setif 1, Setif 19000, Algeria
[d] Department of Chemistry, Faculty of Sciences, University of M'sila, University Pole, Road BourdjBouArreiridj, M'sila 28000, Algeria
[e] Department of Physics, College of Science, Taif University, Taif 21944, Saudi Arabia
[f] Department of Chemistry, College of Sciences, Northern Border University, P.O. Box 1321, 91431, Arar, Saudi Arabia
[g] Faculty of Educational Sciences, Al-Ahliyya Amman University, Amman 19328, Jordan
[h] Department of Biosciences, Saveetha School of Engineering, Saveetha Institute of Medical and Technical Sciences, Chennai 602105, India

ARTICLE INFO

*Keywords:*
Polyoxymethylene (POM)
Fracture Mechanics
J-Integral
Strain Rate Sensitivity
Mechanical Behavior
Cavitation
Plastic Deformation
Crack Propagation

ABSTRACT

Polyoxymethylene (POM) is a semi-crystalline thermoplastic renowned for its outstanding mechanical strength, wear resistance, and dimensional stability. This study examines the fracture mechanics and mechanical behavior of POM under large deformations using both experimental and numerical approaches. Tensile tests on notched and unnotched specimens reveal a transition from linear elasticity to nonlinear viscoelastic and plastic behavior, with failure mechanisms primarily governed by cavitation and fibrillation. Fracture toughness is assessed using the J-integral method, which demonstrates a strain rate-dependent response. Load-displacement curves show that higher strain rates lead to increased stress thresholds, followed by softening, an extended plateau, and subsequent hardening. Thermal analysis confirms POM's high crystallinity (~40 %) and stability at elevated temperatures. Numerical simulations in ABAQUS validate the experimental findings, emphasizing the role of stress triaxiality in crack propagation and failure mechanisms. The results highlight POM's ductile fracture behavior and provide valuable insights for optimizing its performance in structural and industrial applications. Future research should focus on refining predictive models that integrate plastic deformation and damage evolution to further enhance POM's reliability under extreme conditions.

## 1. Introduction

Through various scholarly works, numerous ongoing questions have been raised regarding the accurate description of brittle material behavior. Among these, studies referenced in [1,2] have contributed significantly to this discourse. It is widely acknowledged that continuous damage theories are effective in predicting material degradation caused by deformation processes, as well as the initiation of macroscopic cracks. However, while these theories offer a scientific framework for understanding the deterioration of elastic structures, they sometimes fail to accurately depict the progression of cracks and the subsequent mechanisms that result in full fracture. The presence of critical defects defines the worst-case scenarios, which often serve as the determining factors in material failure. Failure risk computation can proceed just when needed. Understanding such critical conditions is essential for reliable and safe design, particularly in structural applications [3].

Several fracture analysis methods have garnered significant attention in the research community. One such approach relies on continuum mechanics principles, which assume the presence of a prime flaw. This approach allows for the prognosis of how defects evolve under specific loading conditions and offers a detailed description of mechanical properties near the crack tip [4]. Alternatively, other descriptive approaches aim to develop simplified numerical models that establish essential criteria for crack initiation [5]. The development of these standards, along with the associated parameters, can differ based on the degree of plastic deformation taking place in the substance. There are

* Corresponding author.
*E-mail address:* fatmimessaoud@yahoo.fr (M. Fatmi).

https://doi.org/10.1016/j.mtcomm.2025.114411
Received 17 September 2025; Received in revised form 25 November 2025; Accepted 27 November 2025
Available online 28 November 2025

several techniques and standards available for determining the linear elastic fracture mechanics factors for polymers under crack and plane strain conditions, as well as for low and moderate loading levels [6–10]. In a variety of mechanical applications including water, gas, and oil pipelines, rockets, turbojets, and even biomechanics such as blood arteries and thin tubes the use of cylindrical polymer structures has grown in popularity. Nevertheless, extremely harsh working conditions such as internal and external stresses are frequently applied to these structures. There is a potential for catastrophic collapse since these structures can deform significantly under the influence of stress, internal pressures, or temperature changes [11]. The molecular deformation mechanisms of semi-crystalline polymeric materials are well understood, yet it is challenging to ascertain their macroscopic impacts. The polymer is treated as a linear viscoelastic material under vibrational loading and as a linear elastic substance under static loading when subjected to very small deformations. It is distinguished by a non-linear viscoelastic behavior for larger deformations. The polymer may alternatively be regarded as a plastic or even a visco-plastic substance during these significant deformations [12]. To describe nonlinear deformation, many studies have used plasticity theory as a convenient framework [13–19]. Additional investigations [20–25] have shown that the integrity of the fractured specimen can be evaluated through experimental and numerical validation of fracture models. There is constant notification of mechanical fractures everywhere. All fracture modes are covered in the design processes of current structural codes. A key parameter in fracture analysis is the determination of a reduction factor that quantifies the loss of strength in the presence of a defect or notch a concept that is also relevant to polymeric materials such as POM. Considering the aforementioned challenges in fracture prediction and the need for reliable modeling of polymeric materials, this study focuses on the mechanical and fracture behavior of POM through combined experimental and numerical approaches. In this work, particular attention is given to the effects of strain rate, damage mechanisms, and fracture energy evaluation using the J-integral method. The proposed approach aims to establish a consistent framework for assessing the toughness and deformation behavior of POM under various loading conditions. We characterize the POM rupture using global approaches, specifically the J integral. Furthermore, the resistance force J-R can be constructed thanks to the parameter J. To find cracks or other flaws in POM, we need to follow a certain process. This study is essential for understanding the fracture mechanics and mechanical behavior of polyoxymethylene (POM) under large deformations, providing valuable insights into its strength, failure mechanisms, and strain rate sensitivity. The findings contribute to optimizing POM for industrial applications, including automotive components, aerospace structures, medical devices, and industrial machinery. By improving the material's reliability and durability, this research supports advancements in manufacturing, structural engineering, and high-performance polymer applications. Recent developments in polymer and composite fracture mechanics have emphasized the interplay between strain rate, microstructural design, and energy dissipation. Wang et al. [26] analyzed the visco-hyperelastic response of isotropic liquid crystal elastomers, while Zhao et al. [27] demonstrated the rate-dependent fracture behavior of polymeric composites under impact. Zhu et al. [28] introduced discrete assembled metamaterials with tunable plastic energy absorption, and Ji et al. [29] designed biomimetic carbon fiber composites exhibiting superior impact tolerance through optimized Bouligand symmetry. Complementarily, Liu et al. [30] highlighted how microstructural gradients and nanoscale reinforcements govern local stress redistribution and energy dissipation during fracture in metallic–polymeric systems. Collectively, these studies reveal a consistent framework linking strain-rate effects, microstructural tailoring, and energy absorption concepts that underpin the present investigation of POM fracture and toughness behavior.

## 2. Material and methods

### 2.1. Experimental procedures

Tensile tests were carried out on both notched and unnotched Polyoxymethylene (POM) specimens to evaluate their mechanical and fracture behavior under different loading conditions. The unnotched tensile specimens were prepared according to ASTM D638 [31] Type I standard, with an overall length of 165 mm, a gauge length of 50 mm, a width of 13 mm, and a thickness of 3 mm. The notched specimens were designed following the ASTM D5045 [32] standard, having a single-edge notch with a notch root radius of 2 mm and a total length of 60 mm. The specimens were machined from extruded POM plates using a CNC milling process, followed by fine polishing to remove any surface irregularities and reduce machining-induced stress concentrations. All tests were conducted at room temperature ($23 \pm 2\ ^{\circ}C$) using a universal testing machine equipped with an extensometer to measure the axial strain accurately. The crosshead speeds corresponded to nominal strain rates of $10^{-3}\ s^{-1}$, $10^{-2}\ s^{-1}$, and $10^{-1}\ s^{-1}$ to investigate the influence of strain rate on the mechanical response. At least three tests were performed for each condition to ensure repeatability. The load–displacement curves were recorded continuously, and the true stress–strain curves were derived for numerical modeling. Fracture surfaces were examined using an optical microscope to identify the dominant failure mechanisms (cavitation and fibrillation) [33].

### 2.2. Numerical simulation

The numerical analysis was performed using ABAQUS 2013 finite element software [34] to simulate the experimental tensile tests and to analyze the local stress and strain distribution around the notch. The POM material was modeled as an elastic–plastic solid with isotropic hardening, assuming constant volume during large deformations, a common assumption for polymers exhibiting significant flexibility [35]. The constitutive behavior was implemented using an elastic–plastic model with isotropic hardening, where the true stress–strain data obtained from experiments were used as input. The material parameters were as follows: Elastic modulus $E = 2.9$ GPa, Poisson's ratio $\nu = 0.35$, and yield stress $\sigma = 65$ MPa. The specimen geometry corresponded to the experimental configuration, modeled as a flat notched tensile bar to replicate the uniaxial stress state, as proposed by Bridgman [35] and further developed by Hill [36] for describing triaxial stress effects in notched specimens. The model used 3D eight-node brick elements (C3D8R) with reduced integration. A refined mesh was applied around the notch region to ensure accurate stress and strain prediction. Symmetric boundary conditions were imposed along the specimen's midplane to reduce computational cost and exploit geometric symmetry [37]. One end of the specimen was fully constrained, while the other was subjected to a uniform axial displacement to simulate tensile loading. Both geometric and material nonlinearities were considered in the analysis. A plane-stress distribution was observed near the specimen surface, consistent with findings from previous studies [38]. The J-integral was calculated along multiple contours around the crack front to evaluate the energy release rate and fracture toughness. Numerical results were compared with the experimental data to validate the model's accuracy. A schematic of the examination swab geometry is shown in Fig. 1a, with a comprehensive stress divide plot in Fig. 1b to precisely characterize the stress distribution in a plane stress state [38] and around the notch.

Assuming that our material behaves as a perfect elastic-plastic, Numerical emulation were performed on a swab subjected to stretchy loading (Fig. 2) to investigate the mechanical attitude of polymers under significant distortion. The majority of polymer materials do not fit this premise due to their large deformations. Many authors [37–45] have supported the utilize of that model type to determine rupture strength founded on the incremental J integral and indoor power intensity.

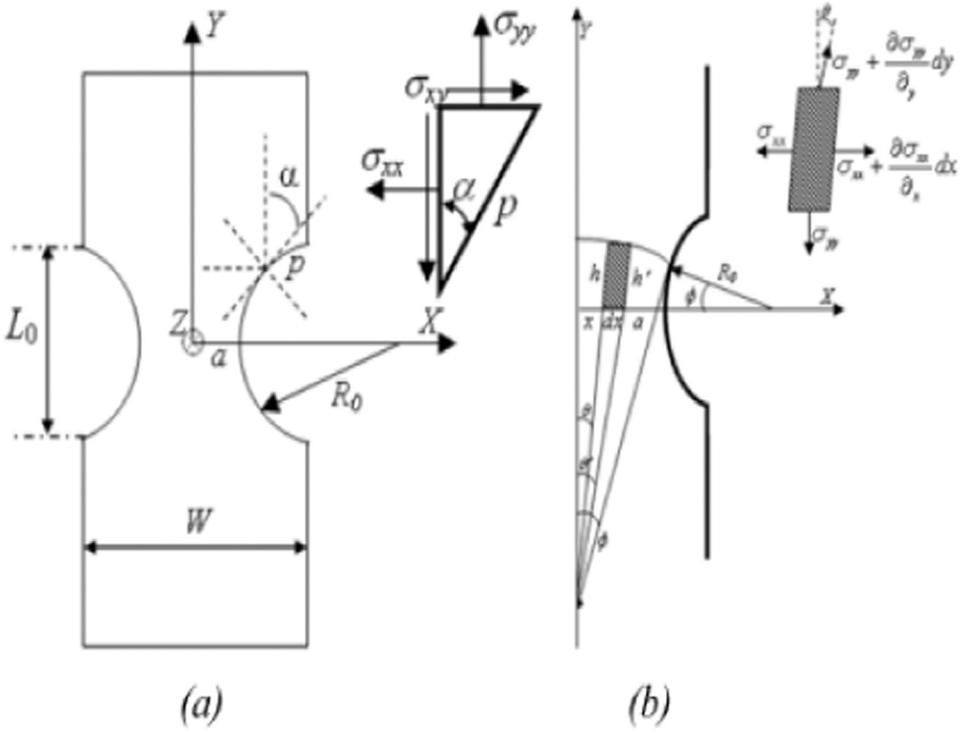


**Fig. 1.** Schematic representation of the notched specimen and stress components near the notch root. (a) Geometry of the specimen, (b) Local stress distribution.

The load evolution in uniaxial traction as a function of POM displacement is shown in Fig. 3. These tests are conducted under various real strain rates and at a temperature of 23°C. We can see from the figure that the load F increases with the strain speed. Beyond this threshold, we observe a less pronounced softening that is followed by a lengthy plateau that culminates in the start of hardening. The energy parameter J is the first global method we suggest using to describe the fracture of our material. Rice [46,47] developed concept of the contour integral J, is an energy-based. It represents the rate of mechanical energy release at each point under static loading, as indicated by its local value Fig. 4.

$$J = \lim \int_{\Gamma} \left( W n_1 - \sigma_{ij} \frac{\partial u_i}{\partial x} n_j \right) d\Gamma \tag{2}$$

$$W = \int_0^{\varepsilon_{ij}} \sigma_{ij} d\varepsilon_{ij} \tag{3}$$

Where Γ is an extremely small contour in the normal plane to the crack front and nj is the normal unit vector at the contour Γ, W is the deformation energy density, $\sigma_{ij}$ is the component of the nominal stress tensor, up is the vector displacement, and $X_1$ is the local cartesian coordinate system at locations on the crack front.

The load evolution in uniaxial traction as a function of POM displacement is shown in Fig. 3. These tests are conducted under various real strain rates and at a temperature of 23°C. We can see from the figure that the load *F* increases with the strain speed. Beyond this threshold, we observe a less pronounced softening that is followed by a lengthy plateau that culminates in the start of hardening. The energy parameter *J* is the first global method we suggest using to describe the fracture of our material Rice [46] developed concept of the contour integral J, is an energy-based. It represents the rate of mechanical energy release at each point under static loading, as indicated by its local value Fig. 4.

$$J_{pl} = -\frac{1}{B} \frac{dU_{pl}}{da} \tag{4}$$

Where *B* represents the thickness of the specimen, a is the length of the crack, and $U_{pl}$ is the plastic potential energy.

Upl represents the plastic potential energy, A denotes the crack length, and B is the specimen's thickness. Begley and Landes [48] demonstrated the empirical evaluation of the J integral using the load-displacement curve, showing its applicability for a rigid down an applied load F or imposed displacement Δ. This method requires the use of multiple specimens. The results of a fracture test, measured using the J integral, include the critical value near the onset of crack evolution and the crack resistance (J-R) curve. As illustrated in Fig. 5, the resistance to crack extension at the crack tip under plane strain conditions corresponds to the high value of J, known as the plane strain crack toughness JIc [49]. However, in the present study, a stable critical value JIc could not be determined under the given testing conditions. This limitation is primarily related to the deformation and fracture mechanisms of POM. Because POM is a semi-crystalline polymer with viscoelastic–plastic behavior, it does not exhibit a well-defined steady-state crack propagation region under the current loading conditions. The material tends to undergo unstable crack growth shortly after initiation, driven by the rapid release of stored elastic energy. As a result, the J–R curve does not reach a plateau, preventing a reliable estimation of the critical value JIc. This behavior has been reported for several semi-crystalline polymers, where the fracture process zone evolves quickly, and the time-dependent relaxation limits the establishment of stable crack growth. Therefore, only comparative or method-dependent J values can be used to assess the fracture toughness of POM under these conditions. To achieve a valid JIc determination, additional experiments under slower strain rates or elevated temperatures are recommended, as these conditions promote more stable crack growth and reduce the influence of viscoelastic effects.

The fracture energy is ultimately characterized by the region under the fload-displacement curve. However, the literature claims that the elongation and crack length findings produced by these techniques are extremely brief. As a result, their application in polymers is still somewhat restricted. Using the following relation, Begley et *al.* [48] suggested an additional technique to calculate the J parameter for each type of specimen based on the measurement of the initial crack length and the wasted energy:

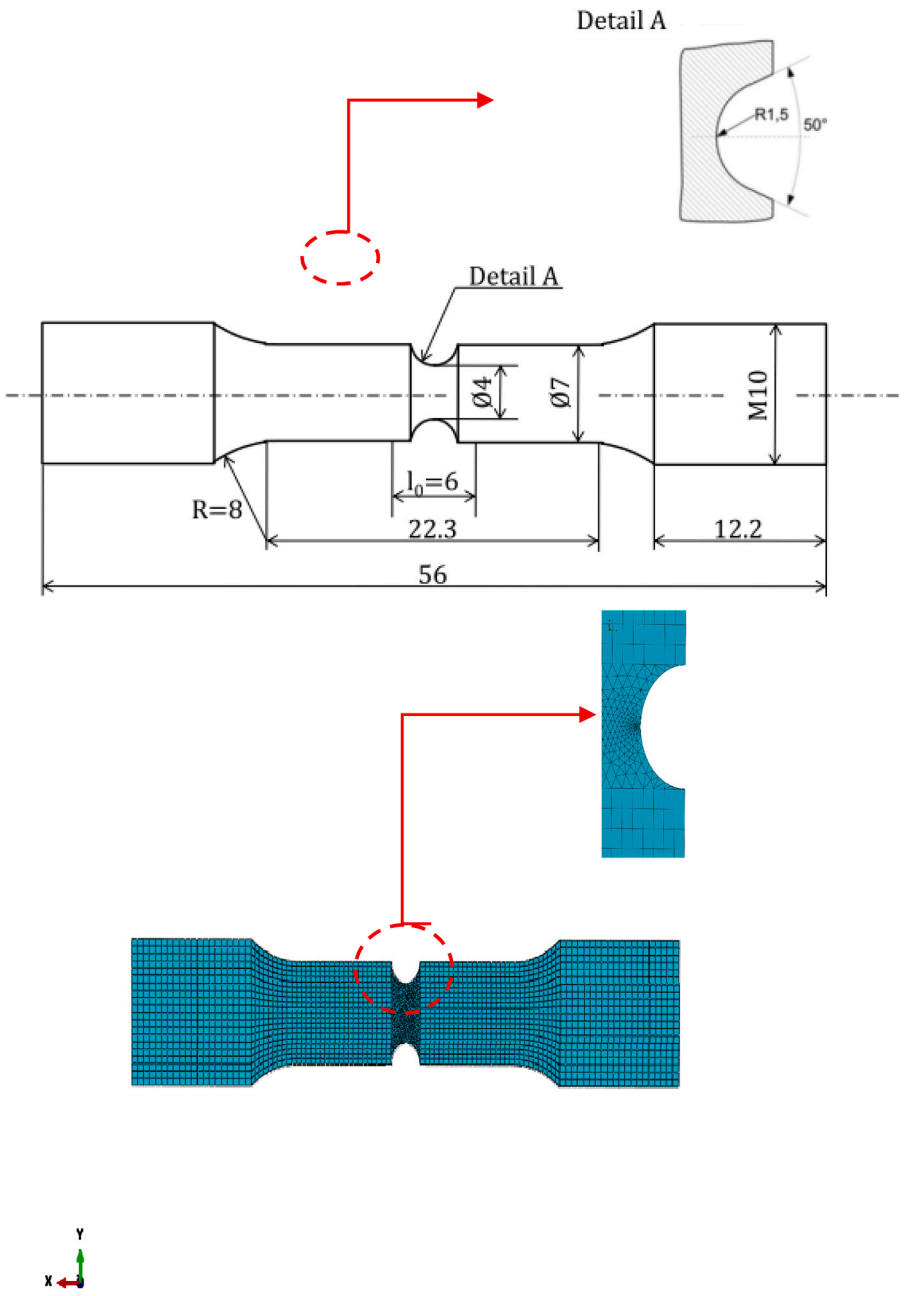


**Fig. 2.** Geometry and finite element model of the notched specimen used in the tensile tests.

$$J = \frac{\eta U}{B(W-a)} \tag{5}$$

Where $\eta$ is a parameter defined by Rice et *al.* [50], and Clarke and Landes [51].

Begley et *al.* [48] expressed the $J$ parameter in the case of elastic-plastic materials as an additive form of two components. An elastic energy ($J_{el}$) and a plastic energy ($J_{pl}$) in the following form:

$$J = J_{el} + J_{pl}$$

where

$$J_{el} = \frac{\eta_{el} U_{el}}{B(W-a)} \text{ and } J_{pl} = \frac{\eta_{pl} U_{pl}}{B(W-a)} \tag{6}$$

where $\eta_{el}$ and $\eta_{pl}$ are the elastic and plastic proportionality Factors influenced by the geometry of the taking and $U_{el}$ and $U_{pl}$ are the elastic and plastic potential energies. It is possible to calculate the elastic component Jel directly from the stress intensity factor K because it is equal to the energy release rate G. To determine the two proportionality factors, $\eta_{el}$ and $\eta_{pl}$, another approach has been suggested. We focus only on the method used by Sharobeam and Landes [49] to calculate the plastic factor (ηpl). This approach is grounded in the theory of charge isolation.

To accomplish so, Bridgman [49] proposed a link between displacement and load for a broken specimen. This relationship is given by the following equation:

$$\theta = F\frac{M}{b^2} \tag{7}$$

Where θ is the rotation brought on by the presence of the fracture, b is the length of the uncracked ligament, and M is the bending moment.

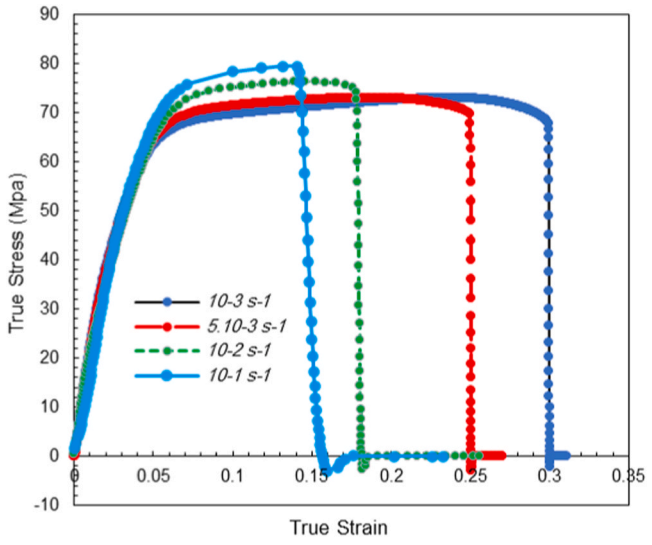


**Fig. 3.** Load–displacement curves of POM specimens tested at room temperature (23 ± 2 °C) under different nominal strain rates.

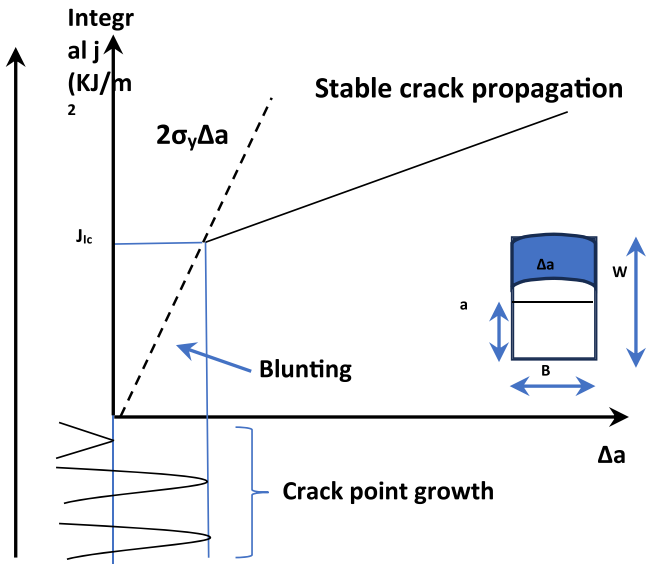


**Fig. 5.** Schematic of the ductile tearing process.

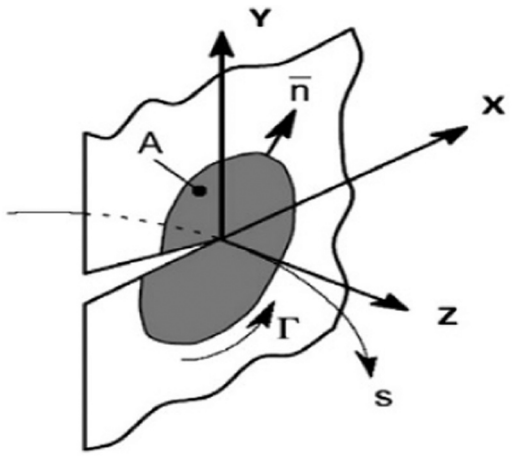


**Fig. 4.** Schematic representation of the integration contour used for the J-integral calculation.

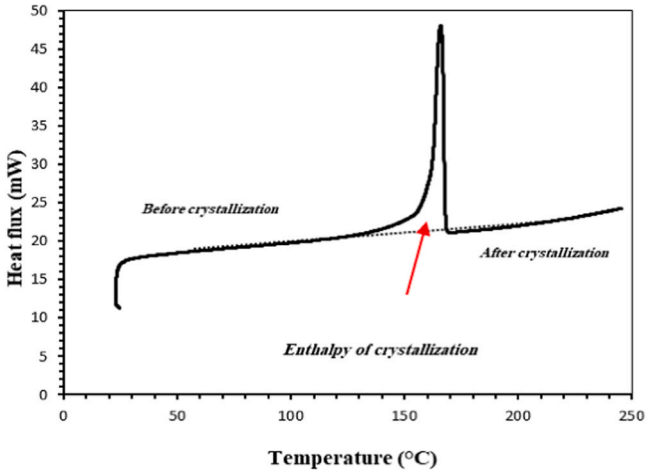


**Fig. 6.** Differential Scanning Calorimetry (DSC) thermogram of the POM specimen.

## 3. Results and discussion

In a nitrogen environment, Differential Scanning Calorimetry (DSC) is used to measure the degree of crystallinity (Xc) of POM. The Perkin-Elmer DSC Diamond device is used to do the DSC measurement at a heating rate of 10 °C/min. To determine the degree of crystallinity (Xc), the following formula is used:

$$X_c = \frac{\Delta H}{\Delta H_0} \tag{8}$$

The enthalpy of fusion measured during the DSC analysis is denoted as ΔH, while the enthalpy of fusion for fully crystalline POM is represented by $\Delta H_0$. The melting point ($T_m$) was also determined using the DSC technique and corresponds to the peak's maximum value. The thermograms for the three positions are presented in Fig. 6. Based on the calculations, the degree of crystallinity (Xc) of POM is approximately 40 %.

During the DSC analysis, we observed that this method provides essential thermal properties, including melting temperature, crystallization temperature, and crystallization rate. According to the reference documents, fracture toughness evaluations were performed using a loading rate equivalent to W/10. To characterize the key features of the polymer fracture model and validate the calculation technique employed for toughness assessment, we first analyze the progression of load-displacement curves. These plots, derived from calculations, correspond to samples with different crack size ratios (a/W), as illustrated in Fig. 7.

The computation software is the source of these curves. For every fracture length taken into consideration, we see comparable changes in the load as a function of displacement, namely a reduction in stiffness and an increase in maximum loads as the crack length increases. Increasing the fracture size from a/W = 0.15 to a/W = 0.25 affected the highest force that could be achieved. Additionally, it had an impact on the sample's total displacement following the maximum load (related to the spread of ductile tearing).

For a given displacement or critical load, the strain energy release rate per unit thickness is commonly used to assess the toughness of a material. The challenge, therefore, lies in determining this energy using the Begley-Landes method [48] with multiple samples. This fracture energy corresponds to the area under the load-plastic displacement curve, as illustrated in Fig. 8.

The graphical representation in Fig. 9 illustrates the variation of plastic energy relative to sample thickness ($U_{pl}$/B) as a function of crack

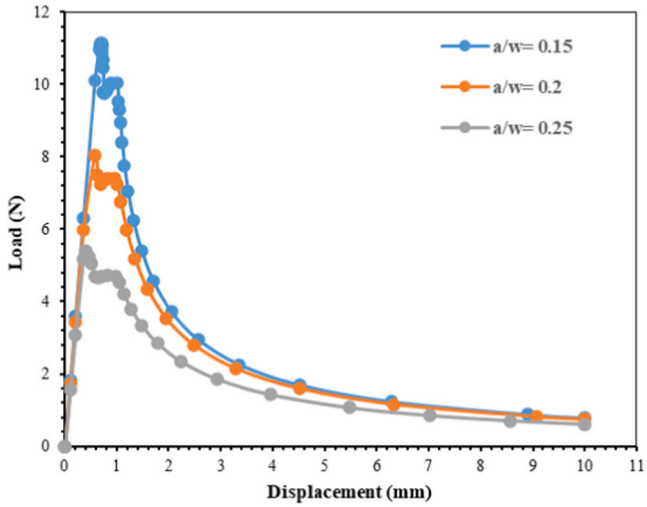


**Fig. 7.** Load–displacement curves for POM specimens with different normalized crack lengths.

length. At first glance, the energy progression appears linear for different comparable plastic displacement values. However, our analysis reveals that both the applied displacement and the initial crack length influence the plastic energy. This dependency enables the calculation of the resulting slope, which corresponds to the crack propagation rate. Furthermore, the introduction of the separation parameter ($\eta_{pl}$) as a function of the ratio (b/W) is depicted in Fig. 10a, where similar trends are observed for the three evaluated crack lengths. As previously discussed, to determine the plastic shape factor ($\eta_{pl}$), a logarithmic integration was performed between the separation parameter ($S_{ij}$) and the ratio (b/W). These evolutions are shown in Fig. 10b, where the plastic shape factor ($\eta_{pl}$) corresponds to the slope of each linear fit. In addition, the stress triaxiality parameter ($\eta$) was quantitatively evaluated to better understand its influence on the deformation and fracture mechanisms of POM. This parameter is defined as $\eta = \sigma_m / \sigma_{eq}$, where $\sigma_m$ represents the hydrostatic stress and $\sigma_{eq}$ is the equivalent von Mises stress. ABAQUS simulation results revealed that $\eta$ increases significantly near the notch root, reaching values between 0.6 and 0.9 depending on the applied strain rate and notch radius. This increase in triaxiality enhances hydrostatic tension, promoting void nucleation and accelerating cavitation processes. Conversely, regions with lower $\eta$ values exhibited more homogeneous plastic flow and delayed crack initiation. The observed correlation between triaxiality gradients and fracture morphology confirms that local stress states govern the transition from plastic deformation to ductile tearing in POM. These findings establish a direct link between stress triaxiality, plastic energy dissipation, and the onset of fracture under tensile loading.

With all this information, we can finally plot the evolution of the J-integral with the different methods mentioned previously and with the numerically obtained values. As previously mentioned, the standard provides several techniques for determining the J-integral based on the load-displacement curve. Fig. 11 presents the evolution of the load and the corresponding J-integral values for each crack length. These values were obtained using the two methods proposed in this study, as well as the calculation software, as a function of plastic displacement. Fig. 12 shows the results obtained for $J_M$ with all the different fracture lengths using three different integration strategies. It appears that the fracture length has little effect on the utility of $J_M$ when looking at each method independently. However, we see that the values produced by each method vary greatly. Therefore, even if JM is affected by the geometry and test type (and therefore by the loading circumstances), we conclude that it is not an intrinsic property of the material.

The observed differences in J-integral values obtained using various computational approaches can be explained by the viscoelastic–plastic

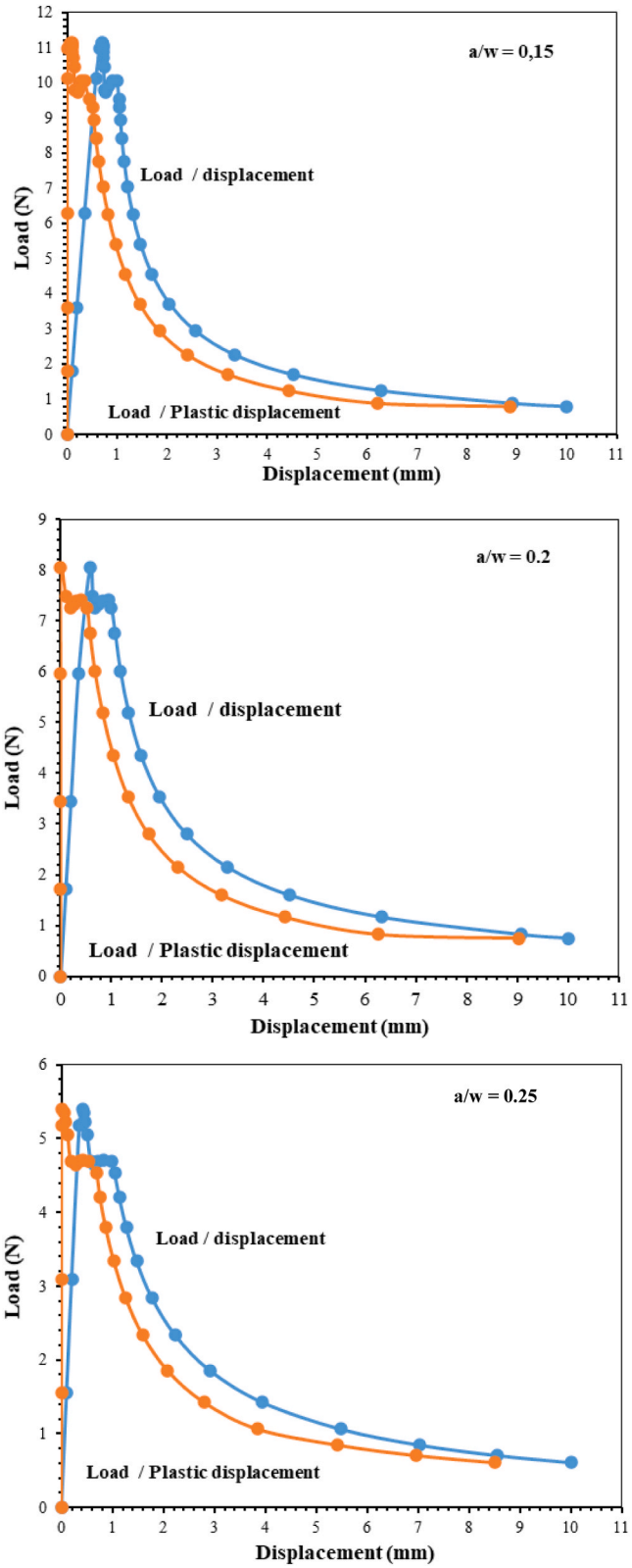


**Fig. 8.** Comparison between total and plastic load–displacement curves for POM specimens with different normalized crack lengths: a/W = 0.15, 0.20, and 0.25.

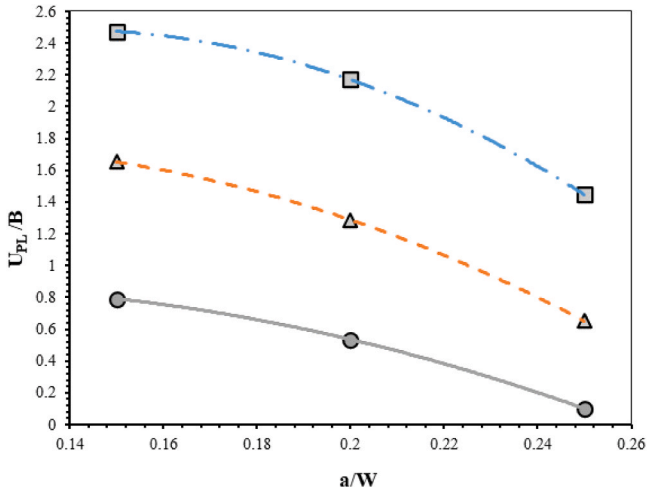


**Fig. 9.** Variation of normalized plastic energy *Upl/B* as a function of the normalized crack length (a/W) for POM specimens.

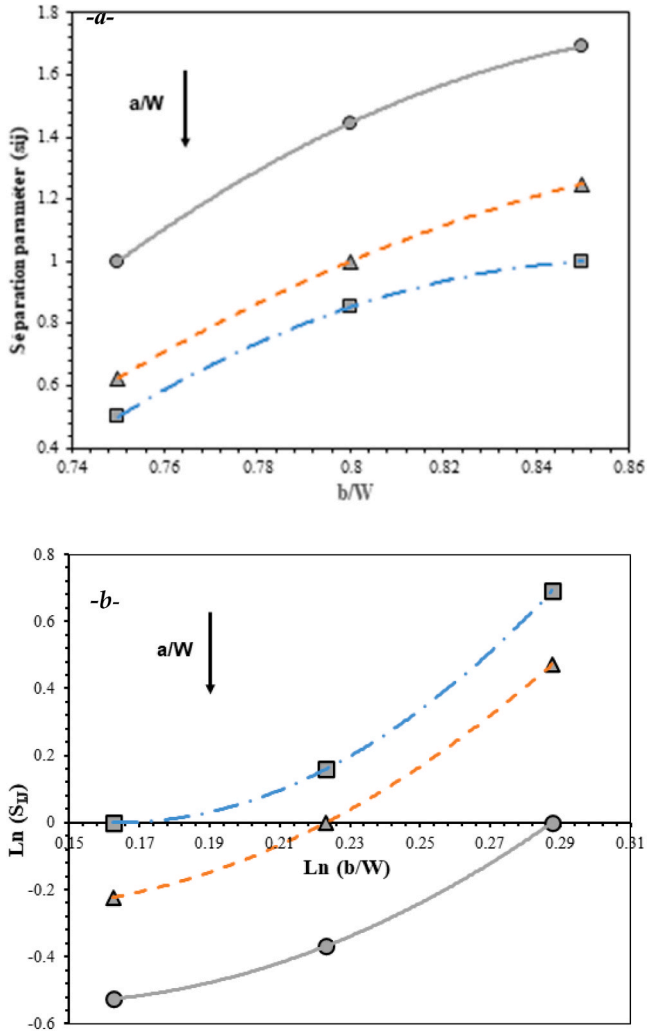


**Fig. 10.** The evolution of the separation parameter Sij and its logarithmic transformation (lnSij) as a function of the ratio (b/W).

nature of POM and its sensitivity to strain rate. Since POM is a semi-crystalline polymer, its deformation involves multiple energy dissipation mechanisms, including molecular chain uncoiling, localized

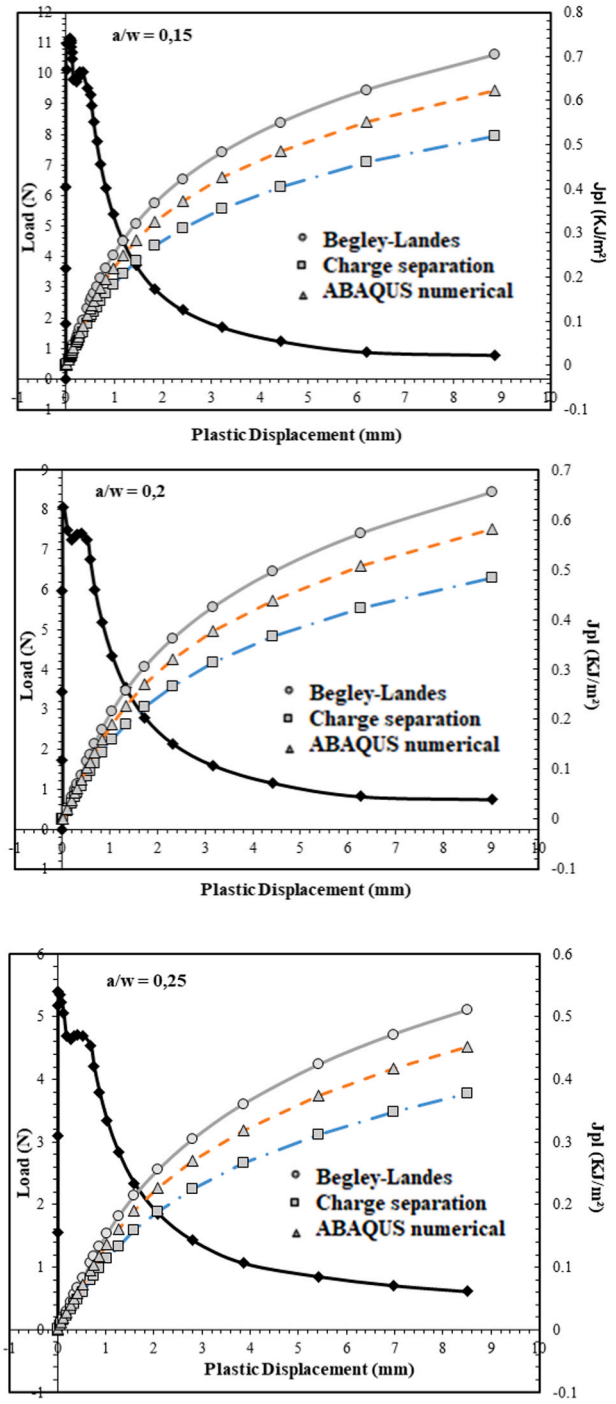


**Fig. 11.** Comparison of load and J-integral evolution as a function of plastic displacement for different normalized crack lengths: a/W = 0.15, 0.20, and 0.25.

cavitation, and micro-void growth. These processes alter the local stress–strain distribution near the crack tip and consequently affect the evaluated J values. In methods that assume purely elastic–plastic behavior, the energy release rate tends to be underestimated because the time-dependent viscoelastic contribution is neglected. Conversely, approaches incorporating nonlinear viscoelastic effects predict higher J values due to additional energy absorption. Therefore, the J-integral obtained under these conditions is method-dependent and cannot be regarded as an intrinsic material property, which aligns with previous findings for other engineering polymers under similar conditions. In

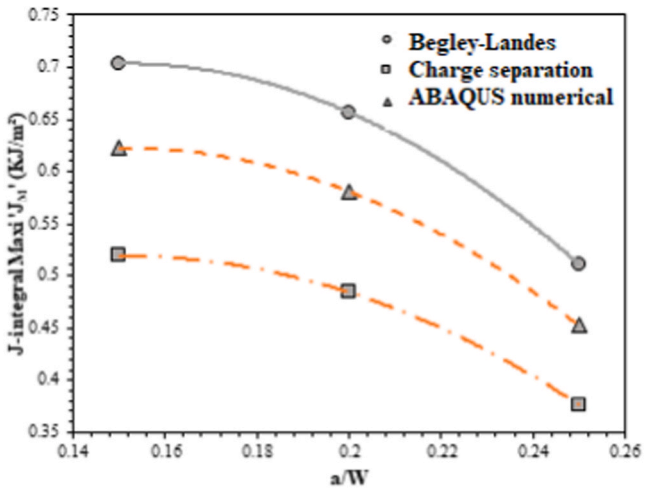


**Fig. 12.** The variation of the mean J-integral value ($J_m$) with normalized crack length (a/W) and ABAQUS numerical methods.

particular, when comparing the Begley–Landes formulation, the charge-separation approach, and the ABAQUS numerical simulation (Figs. 11–12), a consistent trend is observed. The Begley–Landes method, based on a purely elastic–plastic assumption, yields lower J values, whereas the charge-separation and ABAQUS methods—which incorporate nonlinear viscoelastic effects—produce higher J estimates. This consistency across experimental and numerical analyses reinforces that JM is not an intrinsic material constant but a response parameter influenced by strain rate, plastic dissipation, and viscoelastic energy storage. Consequently, a rigorous fracture toughness assessment of semi-crystalline polymers such as POM must integrate both time-dependent and plastic energy contributions to capture the true material resistance. Fig. 13; illustrates the elastic correction factor as a function of all considered fracture lengths. For each technique applied independently, the evolution of this factor appears to follow a linear trend. However, it was observed that the values of ηel are influenced by the crack length, indicating a dependency on specimen geometry and loading conditions. Fig. 14; illustrates the evolution of the energy-displacement curve obtained numerically, depicting the crack progression in a specimen with a width of B= 10 mm. The curves exhibit a consistently increasing trend. Notably, for a displacement increase of approximately 1 mm, a reduction in the gap between the curves ranging from 0.01 to 0.2 is observed. Additionally, the energy evolution with displacement follows a similar

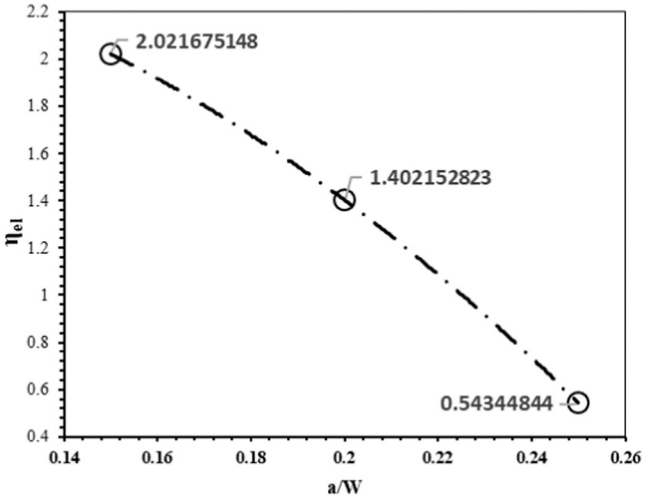


**Fig. 13.** The evolution of the elastic proportionality factor ($\eta_{el}$) as a function of the normalized crack length (a/W).

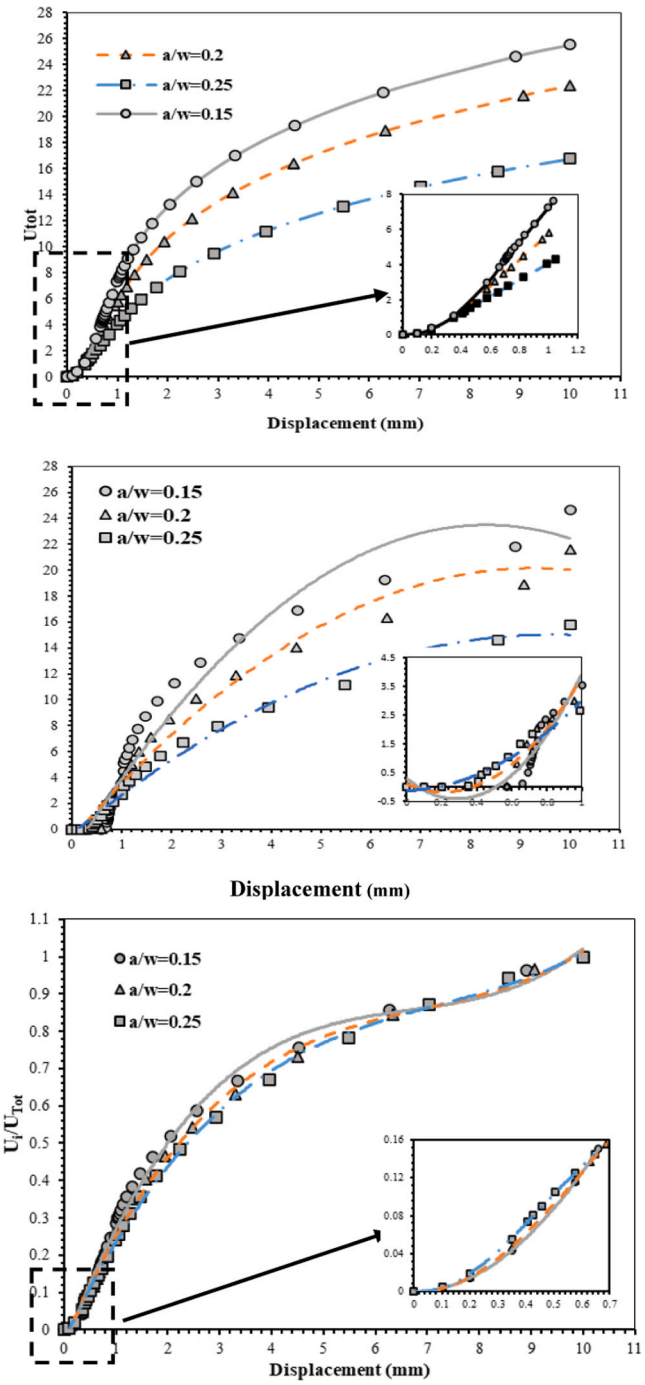


**Fig. 14.** Evolution of total energy ($U_{t_ot}$), plastic energy ($U_{pl}$), and the energy ratio ($U_{pl}/U_{t_ot}$) as a function of displacement for different normalized crack lengths (a/W = 0.15, 0.20, 0.25).

pattern for all considered crack lengths, characterized by a decrease in stiffness and maximum loads as the crack length increases.

## 4. Conclusions

This study aimed to characterize and analyze the mechanical behaviour of polyoxymethylene (POM) under various mechanical conditions, including plastic energy variation, stress triaxiality effects, and fracture modelling factors that remain relatively unexplored for this semi-crystalline material under large deformations. Numerical approaches were employed to investigate POM's deformation, fracture

mechanisms, and damage evolution. The results revealed significant macroscopic transformations under different stress triaxialities, with high ductility and pronounced plastic energy variations. Cavitation was identified as the primary damage mechanism. To further examine stress triaxiality effects, tensile tests on notched specimens were conducted, allowing for an assessment of ductile fracture criteria. The findings demonstrated a strong correlation between numerical and experimental data, particularly in stress-plastic energy relationships and load-displacement responses of fractured specimens. Additionally, the J-integral approach was validated for global fracture analysis, though JIC values could not be directly determined due to the absence of crack initiation in the tested geometry.

## Funding

The authors extend their appreciation to Taif University, Saudi Arabia, for supporting this work through project number (TU-DSPP-2024–63).

## CRediT authorship contribution statement

**Sid Ahmed Reffas:** Conceptualization. **R. Yekhlef:** Conceptualization. **D. Belfennache:** Data curation. **Fatmi M:** Validation, Data curation. **Ghebouli M.A.:** Data curation. **S. Alomairy:** Conceptualization. **Mustafa Jaipallah Abdelmageed Abualreish:** Data curation. **Aseel Smerat:** Formal analysis.

## Declaration of Competing Interest

The authors declared no potential conflicts of interest with respect to the research, authorship, and/or publication of this article.

## Data availability

No data was used for the research described in the article.

## References

[1] Z.P. Bazant, C.G. Pijaudier, Nonlocal continuum damage, localization, instability and convergence, ASME J. Appl. Mech. 55 (1988) 287–293.
[2] H.C. Mattos, M. Fremond, E.N. Mamiya, A simple model of the mechanical behavior of ceramic-like materials, Int. J. Solids Struct. 29 (24) (1992) 3185–3200.
[3] J.G. Williams, Fracture mechanics of polymers, Polym. Eng. Sci. 17 (1977) 144–149.
[4] S.A. Reffas, M. Benguidiab, O. Sikula, H. Adjlout, H. Lebbal, Numerical study of cracking a medium elastic-viscoplastic polyacetal, Mech. Mech. Eng. 23 (2019) 125–129.
[5] B. Bahrami, M.R. Ayatollahi, A.R. Torabi, Predictions of fracture load, crack initiation angle, and trajectory for V-notched Brazilian disk specimens under mixed mode I/II loading with negative mode I contributions, Int. J. Damage Mech. 27 (8) (2018) 1173–1191.
[6] F.M. Peres, C.G. Schön, J.R. Tarpani, Effect of precracking method on KIc results for medium-density polyethylene tested under cryogenic condition, Polym. Test. 29 (6) (2010) 667–673.
[7] S. De, M. Joelmir, H.N. Yoshimura, F.M. Peres, G.S. Cláudio, Effect of sample pre-cracking method and notch geometry in plane strain fracture toughness tests as applied to a PMMA resin, Polym. Test. 31 (6) (2012) 834–840.
[8] A.B. Martínez, N. León, D. Arencon, J. Rodriguez, A. Salazar, On the effect of the different notching techniques on the fracture toughness of PETG, Polym. Test. 32 (7) (2013) 1244–1252.
[9] E. Bura, A. Seweryn, Mode I fracture in PMMA specimens with notches – Experimental and numerical studies, Theor. Appl. Fract. Mech. 97 (2018) 140–155.
[10] A. Salazar, J. Rodriguez, F. Arbeiter, G. Pinter, A.B. Martínez, Fracture toughness of high density polyethylene: Fatigue pre-cracking versus femtolaser, razor sharpening and broaching, Eng. Fract. Mech. 149 (2015) 199–213.
[11] R. Zerrouki, A. Karas, M. Zidour, A. Bousahla, A. Tounsi, F. Bourada, K. Benrahou, S.R. Mahmoud, Effect of nonlinear FG-CNT distribution on mechanical properties of functionally graded nanocomposite beam, Struct. Eng. Mech. 78 (2) (2021) 117–124.
[12] L. Belec, Mise en évidence de la contribution des phases amorphe et cristalline du polyamide de la transition vitreuse, Thèse Univ. De. Poitiers (1995).
[13] C. Andriss, A. Kenf, T. Donhauser, S. Schmeer, Characterization and modeling of continuous carbon fiber-reinforced polycarbonate under multiaxial loads, Compos. Part B Eng. 235 (2022) 109740.
[14] T. Laux, K.W. Gan, J.M. Dulieu-Barton, O.T. Thomsen, A simple nonlinear constitutive model based on non-associative plasticity for UD composites: development and calibration using a modified arcan fixture, Int. J. Solids Struct. 162 (2019) 135–147.
[15] J.F. Chen, E.V. Morozov, K. Shankar, A combined elastoplastic damage model for progressive failure analysis of composite materials and structures, Compos. Struct. 94 (12) (2012) 3478–3489.
[16] T. Yokozeki, T. Ogasawara, T. Ishikawa, Nonlinear behavior and compressive strength of unidirectional and multidirectional carbon fiber composite laminates, Compos. Part A Appl. Sci. Manuf. 37 (11) (2006) 2069–2079.
[17] M. Rezaiee-Pajand, M. Sharifian, A novel formulation for integrating nonlinear kinematic hardening Drucker-Prager's yield condition, Eur. J. Mech. A/Solids 31 (1) (2012) 163–178.
[18] L. Szabó, A. Kossa, A new exact integration method for the Drucker–Prager elastoplastic model with linear isotropic hardening, Int. J. Solids Struct. 49 (1) (2012) 170–190.
[19] C. Hoffarth, S.D. Rajan, R.K. Goldberg, D. Revilock, K.S. Carney, P. DuBois, G. Blankenhorn, Implementation and validation of a three-dimensional plasticity-based deformation model for orthotropic composites, Compos. Part A Appl. Sci. Manuf. 91 (2016) 336–350.
[20] A.B. Martínez, N. León, A. Segovia, J. Cailloux, P.P. Martínez, Effect of specimen notch quality on the essential work of fracture of ductile polymer films, Eng. Fract. Mech. 180 (2017) 296–314.
[21] N. León, A.B. Martínez, P. Castejón, P.P. Martínez, D. Arencón, Notch effect on the fracture of a polymeric film, Theor. Appl. Fract. Mech. 95 (2018) 270–282.
[22] M. Lorenzo-Bañuelos, A. Díaz, I.I. Cuesta, Influence of raster orientation on the determination of fracture properties of polypropylene thin components produced by additive manufacturing, Theor. Appl. Fract. Mech. 107 (2020) 102536.
[23] A.B. Martínez, N. León, D. Arencón, M. Sánchez-Soto, Essential work of fracture, crack tip opening displacement, and J-integral relationship for a ductile polymer film, Polym. Test. 55 (2016) 247–256.
[24] A.B. Martínez, N. León, D. Arencón, M. Sánchez-Soto, The post-yield fracture of a ductile polymer film: notch quality, essential work of fracture, crack tip opening displacement, and J-integral, Eng. Fract. Mech. 173 (2017) 21–31.
[25] A.B. Martínez, A. Segovia, J. Gamez-Perez, M.L. Maspoch, Influence of femtolaser notch sharpening technique in the determination of essential work of fracture (EWF) parameters, Eng. Fract. Mech. 76 (9) (2009) 1247–1254.
[26] X. Wang, J. Han, H. Xu, H. Ji, Z. Yue, R. Zhang, B. Li, Y. Ji, Z. Li, P. Wang, T.J. Lu, Nonlinear mechanical behaviour and visco-hyperelastic constitutive description of isotropic-genesis, polydomain liquid crystal elastomers at high strain rates, J. Mech. Phys. Solids 193 (2024) 105882.
[27] X. Wang, H. Ji, X. Li, S. Sun, Q. Zhang, V.P.W. Shim, T.J. Lu, Static and dynamic compressive and tensile response of highly stretchable polyurea, Int. J. Impact Eng. 166 (2022) 104250.
[28] N. Zhu, Y. Xu, X. Wang, X. Xu, Z. Yue, X. Guo, H. Ji, B. Li, Y. Ji, Z. Li, P. Wang, Plastically isotropic mechanical metamaterials with discrete assemblies, Adv. Funct. Mater. 35 (29) (2024) 2424390.
[29] H. Ji, X. Wang, B. Li, Z. Yue, X. Xu, R. Zhang, Z. Li, H. Meng, T.J. Lu, P. Wang, Mid-plane symmetrical Bouligand structural design for robust multi-impact resistance, Adv. Funct. Mater. (2025).
[30] R. Yu, X. Li, Z. Yue, A. Li, Z. Zhao, X. Wang, H. Zhou, T.J. Lu, Stress state sensitivity for plastic flow and ductile fracture of L907A low-alloy marine steel: from tension to shear, Mater. Sci. Eng. A 835 (2022) 142689.
[31] ASTM D638, Standard test method for tensile properties of plastics. ASTM Int., West Conshohocken, PA, (2014).
[32] ASTM D5045, Standard test method for plane-strain fracture toughness and strain energy release rate of plastic materials. ASTM Int., West Conshohocken, PA, (2014).
[33] A.J. Kinloch, R.J. Young, Fracture behaviour of polymers, Springer, London, 1995.
[34] ABAQUS, Analysis User's Manual. Version 6, Dassault Systemes Simulia Inc., (2013).
[35] P.W. Bridgman, The stress distribution at the neck of a tension specimen, Trans. ASM 32 (1944) 553–574.
[36] R.H. Hill, On the discontinuous plastic states with special reference to localized necking in thin sheet, J. Mech. Phys. Solids 1 (1952) 19–30.
[37] B. Cotterell, T. Pardoen, A.G. Atkins, Measuring toughness and the cohesive stress–displacement relationship by the essential work of fracture concept, Eng. Fract. Mech. 72 (6) (2005) 827–848.
[38] L. Gori, S.S. Penna, R.L. Da Silva Pitangueira, Discontinuous failure in micropolar elastic-degrading models, Int. J. Damage Mech. 27 (10) (2018) 1482–1515.
[39] L. Lu, S. Wang, An analytical method to predict residual strength based on critical CTOA, Eng. Fract. Mech. 200 (2018) 31–41.
[40] T. Pardoen, F. Hachez, B. Marchioni, P.H. Blyth, A.G. Atkins, Mode I fracture of sheet metal, J. Mech. Phys. Solids 52 (2) (2004) 423–452.
[41] T. Pardoen, Y. Marchal, F. Delannay, Thickness dependence of cracking resistance in thin aluminium plates, J. Mech. Phys. Solids 47 (10) (1999) 2093–2123.
[42] L. Lu, S. Wang, G. Tong, Relationship between incremental J-integral and crack tip opening angle in elastic-plastic materials, Eur. J. Mech. A/Solids 75 (2019) 399–409.
[43] L. Lu, Z. Liu, T. Wang, Z. Zhuang, An analytical model of fracture process zone to explain why crack-tip opening angle works, Eng. Fract. Mech. 233 (2020) 107054.
[44] L. Lu, Z. Liu, Y. Cui, Z. Zhuang, Driving force on line fracture process zone and fracture parameters suitable for elastic–plastic materials, Int. J. Solids Struct. 217 (2021) 15–26.
[45] S.A. Reffas, M. Elmeguenni, Analysis of void growth and coalescence in porous polymer materials, Eng. Technol. Appl. Sci. Res. 3 (3) (2013) 452–460.

[46] J.R. Rice, Mathematical analysis in the mechanics of fracture, in: H. Liebowitz (Ed.), Fracture: An Advanced Treatise, 2, Academic Press, New York, 1968, pp. 191–311.
[47] L. Rezgani, K. Madani, M. Mokhtari, X. Feaugas, S. Cohendoz, S. Touzain, S. Mallarino, Adhes. Sci. Technol 32 (13) (2018) 1393–1409.
[48] Begley J.A., Landes J.D., The J-integral as a fracture criterion. ASTM STP 514, ASTM, Philadelphia, 1–23, (1972).
[49] M.H. Sharobeam, J.D. Landes, The load separation criterion and methodology in ductile fracture mechanics, Int. J. Fract. 47 (1991) 81–104.
[50] Rice J.R., Paris P.C., Merkle J.G., Some further results of J-integral analysis and estimates. In: Progress in Flaw Growth and Fracture Toughness Testing, ASTM STP 536, ASTM, Philadelphia, 213-245, (1973).
[51] G.A. Clarke, J.D. Landes, Evaluation of the J-integral for the compact specimen, J. Test. Eval. 7 (5) (1979) 264–269.